RSC Advances

ROYAL SOCIETY OF CHEMISTRY

www.rsc.org/advances

Morphological Evolution of Anodic TiO_2 Nanotubes

Yiyi Yang[1], Yuning Li[1,2] and Mark Pritzker[1]*

[1]Department of Chemical Engineering, [2] Department of Chemistry and

Waterloo Institute for Nanotechnology

University of Waterloo, 200 University Avenue West,

Waterloo, Ontario, Canada N2L 3G1

Abstract

An experimental study on the development of TiO_2 nanostructures during anodization in fluoride-ion containing electrolyte has been conducted. The evolution of this nanostructure involves the inward growth of a porous network at the oxide/substrate interface that develops into nanotubes. A new explanation for the formation of these nanotubes during anodization is proposed based on the geometric changes observed. SEM examination reveals that the newer formed portions of the pore space closest to the oxide/substrate interface are larger in diameter than those above which form earlier in the process. This yields a structure in which pores are wider at their bases than at the outer oxide/electrolyte interface and appear to crowd each other in the lower portions as anodization proceeds. Further SEM evidence suggests that excessive crowding eventually causes some pores to degenerate into inter-tube regions and leave behind distinct nanotubes. We propose that this degeneration process is the main driving force for the structural transformations from the initial oxide layer to a network of nanopores and finally to fully developed nanotubes rather than a separate dehydration or dissolution process as proposed by previous researchers. The differences in morphology between anodic TiO_2 films formed in aqueous and ethylene glycol-based electrolytes are explained using the same model.

1. Introduction

Nanostructured titanium dioxide (TiO_2) has attracted extensive research interest over the last few decades because of its potential for use in various applications such as supercapacitors [1], gas sensors [2], photocatalysts [3] and solar cells [4]. One-dimensional TiO_2 nanostructures can be synthesized using a range of techniques including sol-gel, hydrothermal, electrospinning, anodization and templated methods [5]. Among these techniques, anodization offers some additional advantages such as the ease of fabrication, control of nanostructure dimensions and the ability to form ordered arrays without the use of templates.

TiO_2 nanotubes can be formed by anodization in both aqueous and organic electrolytes, typically in fluoride-containing media. The first nanoporous anodic TiO_2 thin film was reported by Zwilling et al in 1999 [6], while ordered TiO_2 nanotube arrays were later fabricated in HF by Gong et al in 2001 [7]. These studies spurred a great upsurge of interest in this topic and significant modifications and improvements of the nanostructure of anodized TiO_2. For example, nanotubes up to a few microns in length have been synthesized using fluoride-containing electrolytes with controlled acidity [8]. Fluoride-free aqueous electrolytes have also been investigated for the preparation of high-aspect ratio TiO_2 nanotubes [9, 10]. On the other hand, the use of non-aqueous electrolytes such as glycerol [11], DMSO and ethylene glycol [12] has enabled the formation of free-standing nanotubular TiO_2 thin films up to a few hundred microns in thickness.

The formation mechanisms of anodic TiO_2 have been extensively investigated [13-17], but certain aspects are still under debate. It has been widely accepted that the formation of TiO_2 nanostructures during anodization occurs via the concomitant oxidation of titanium at the metal/oxide interface and field-assisted dissolution of oxide at the oxide/electrolyte interface [7]. The proposed reactions are as follows:

Oxidation:

$$Ti + 2O^{2-} \longrightarrow TiO_2 + 4e^- \quad (1)$$

Dissolution:

$$TiO_2 + 6F^- + 4H^+ \longrightarrow [TiF_6]^{2-} + 2H_2O \quad (2)$$

Oxygen evolution:

$$2O^{2-} \longrightarrow O_2 + 4e^- \quad (3)$$

The O^{2-} ions that participate in these reactions are produced through the heterolytic scission of water molecules, which is greatly facilitated by the presence of a high electric field [18].

The field-assisted dissolution model has been challenged in recent years by an alternative field-assisted viscous flow mechanism, proposed first for aluminium oxide (AAO) [19, 20] and later for TiO_2 [21] produced by anodization. According to this model, the compressive stresses associated with electrostriction and volume expansion during oxidation cause the oxide to flow laterally from regions directly below the pore bases toward and up along the nanopore or nanotube wall regions. This process is facilitated by the enhanced plasticity of the barrier layer that arises as the film constituents move under the influence of the electric field [22]. Evidence supporting both models has been provided by various research groups [23-25], indicating that both mechanisms are plausible in the case of anodic TiO_2 nanostructures.

Unlike the formation of AAO nanopores, the anodization of titanium usually produces distinct nanotubular structures. Since the above-mentioned field-assisted dissolution and viscous flow models cannot distinguish nanopore formation from nanotube formation, some other phenomenon must be at play during titanium anodization. New models have been put forward to interpret the formation of gaps in ordered TiO_2 arrays, including inter-pore dissolution, hydroxide phase dehydration and the formation of a fluoride-rich layer at the cell boundaries [14, 26-30].

The first of these models proposes that the metallic parts in the middle of the oxide walls also go through the same field-assisted dissolution process after vertical pores are formed, causing pore walls to split. However, this model does not explain why metallic parts would remain within the pore walls since they are more likely to be oxidized by the anodization process [26].

The dehydration model, on the other hand, proposes that the oxide matrix initially consists of a titanium hydroxide phase $Ti(OH)_x$ which is subsequently dehydrated to produce TiO_2, causing shrinkage of the oxide structure and separation into distinct nanotubes [27-30]. The fact that no separated nanotubular structures are formed in AAO is explained by the poorer stability of $Al(OH)_3$ towards dissolution than $Ti(OH)_x$. However, this model has received some

criticism on the basis of TEM images showing the regions of the nanotube structure corresponding to the porous hydroxide to be denser than the compact oxide layer, whereas the model predicts them to be less so [13].

Lastly, according to the fluoride-rich-layer model, the base of the nanostructures contains a much higher amount of fluoride because of the faster inward migration of F^- ions than O^{2-} [31]. As the oxide flows upward during the viscous flow process to form the vertical pore wall, this fluoride-rich layer should move in the vertical direction and form cell boundaries in the middle of the pore wall. This higher fluoride content makes the cell boundaries easier to dissolve, thereby splitting the pore walls and forming well-defined nanotubes [14]. This explanation is supported by energy-dispersive X-ray spectroscopy analyses showing that a significant amount of fluoride is usually found in TiO_2 samples. However, some doubts arise with this model since TiO_2 nanotubes can also form in fluoride-free environments with chloride ions as the substitute [9, 10]. Since chloride species have lower mobility than O^{2-}, a corresponding chloride-rich-layer is unlikely to form during the development of the nanotubular structure to serve as the intermediate of inter-tube spaces [13].

To gain further insight into the formation mechanism of nanotubular TiO_2 structures, we report here an experimental study on the development of their nanostructures from the initial oxide layer to the fully developed nanotubes during anodization in both aqueous and ethylene glycol-based electrolytes containing fluoride-ions. Particular attention is paid to the transition from the nanoporous structures to ordered nanotube arrays during the process. Based on the structural transformations observed, we propose a new explanation for the formation of TiO_2 nanostructures and nanotubes in particular during anodization.

2. Experimental

The anodization experiments were conducted potentiostatically at room temperature in a conventional two-electrode electrochemical cell with a graphite cathode. Titanium foil (Alfa Aesar, 99.5%, 0.25mm-thick) was used as the substrate for oxide film growth. Prior to anodization, the substrate was cleaned by ultrasonication successively in isopropanol, de-ionized (DI) water and acetone. The anodization potential was set and controlled with a DC power supply (PLH-120, Thurlby Thandar Instruments), while the anodization current was measured. The electrolyte was stirred continuously at a constant rate using a magnetic stir bar.

Sample A was anodized in an ethylene glycol solution containing 0.3 wt % NH_4F and 2 vol % H_2O at an applied potential of 60 V, conditions which are known to produce high aspect ratio TiO_2 nanotube arrays with perfect hexagonal packing [12]. Experiments were conducted for different durations ranging from 5 s to 1 h to study the evolution of TiO_2 morphology during the anodization process. As a comparison, complementary sets of experiments were conducted in an aqueous electrolyte containing 0.05M oxalic acid and 0.3 wt% NH_4F as solute at 5 V (Sample B) and 20 V (Sample C) respectively, in order to determine the effect of water and voltage on nanostructure development.

Once anodization was complete, the samples were washed with de-ionized water and then cleaned briefly in de-ionized water in an ultrasonic bath. The morphology of the anodized samples was examined using field emission scanning electron microscopy (FE-SEM) (LEO 1550, Zeiss). Samples were coated with a ~10 nm Au film before SEM study to prevent sample charging under the electron beam.

3. Results and Discussion

3.1 Current-time transients

A typical current-time transient response observed during the initial stages of anodization for all experiments is presented in Figure 1a. The current density is initially high, then rapidly drops to a minimum point (X) followed by a rise to a maximum (Y) and then a slower decline.

The positions of the local minimum and maximum points vary from sample to sample, but the minimum value typically occurs within 3 minutes of anodization and the maximum between 5 and 15 minutes for the anodization conditions used in this study. The shape of the curves is consistent with that reported in the literature [32, 33]. This shape is largely attributed to the change in the morphology and thickness of the oxide film since the changes in the thickness of the titanium substrate and the electrolyte conductivity should have much less effect on the overall resistance.

At the very start of anodization, the electrical resistance of the film rapidly rises due to the formation of an oxide barrier layer and causes the current to decrease over the initial stage of anodization. At the same time, the film becomes more porous as its nanostructured morphology is developing, which tends to lower its resistance to further reaction. When this effect of the porosity becomes stronger than that of the resistance, the current goes through the minimum at X and begins to rise. Finally, once the evolution of the nanostructure of the oxide film is mostly complete, the porosity of the film remains relatively constant while the resistance slowly increases as the nanostructured oxide grows in thickness. This leads to the current maximum at point Y followed by the gradual decline thereafter. The relative effects of the barrier oxide, porosity and long-term growth of the oxide film on the overall film resistance of the substrate are shown in Figure 1b.

3.2 Anodization in ethylene glycol solution containing NH_4F and H_2O

3.2.1 Final morphology

SEM images along the top, bottom and side of the nanotube array formed on Sample A (anodization in ethylene glycol solution containing 0.3 wt % NH_4F and 2 vol % H_2O at an applied potential of 60 V) after one hour of anodization are shown in Figures 2a, b and c, respectively. The bottom and side views of the sample are obtained from the detached oxide film after ultrasonication. The outer surfaces of the TiO_2 nanotubes appear to be smooth (Figure 2c) and the nanotubes form in an almost perfect close-packed hexagonal arrangement with uniform size distribution (Figure 2b). The top of the oxide film is covered by a layer of precipitate in the form of aggregated TiO_2 nanowires, as shown in Figure 2a. This layer can be easily removed by

brief ultrasonication in de-ionized H_2O after anodization. The exposed top surface after cleaning (Figure 2a inset) shows a close-packed array of nanotubes with circular cross-sections. In addition, regularly spaced ridges are observed on the outer surface of the nanotubes, but only along the lower part of the tubes (Figure 2c inset) and not on the upper portions. Since the oxide film grows inward, the upper portions of the tubes are the oldest portions of the nanotubes that remain and have undergone chemical dissolution longest. The observation that ridges do not appear on the upper portions suggests that they dissolve away before the walls themselves disappear. Some previous studies have shown that the formation of these ridges correlates with a local pH burst at the pore bases during tube formation and subsequent current fluctuations, although no general agreement exists on the exact mechanisms for this phenomenon [27, 28].

3.2.2 Evolution of morphology

Four stages in the evolution of the morphology of the oxide film based on geometrical characteristics that form during the anodization of Sample A are shown in the SEM images in Figure 3. For the purpose of this discussion, they are denoted as I-IV. Also included in Figure 3 is a typical current-time transient obtained during anodization, as discussed in Section 3.1. Based on the times at which the stages are observed to occur during the anodization of Sample A, they are superimposed on the transients in order to relate them to the electrode response. The surface morphology of the Ti substrate is shown in Figure 3a as reference.

From the start of the anodization process up to approximately 5 seconds (denoted as Stage I), the oxide film remains mostly planar with shallow depressions visible as slightly darker lines under high magnification (Figure 3b). During this short period denoted as Stage I, the metal surface is rapidly being oxidized, but nanostructure formation is only commencing. In the next stage, small segments of “nanowalls” separated by deeper trenches form and appear as the darker regions in the SEM images (Figure 3c). These separate nanowall segments eventually appear to link up and connect with each other to form a network in Stage III (Figure 3d), which then evolves into an array of circular pores (Figure 3e). Finally, in the fourth stage, the nanopores develop into nanotubes, as shown in Figure 3f. After this point, the shape of the tops of the TiO_2 nanotubes remains largely unchanged as they grow in the vertical direction.

Although the times at which the various stages occur vary depending on the processing conditions, their positions relative to the local maximum and minimum in the current transient curve remain the same.

It is known that the growth of anodic TiO_2 films begins with the formation of an oxide barrier layer [17, 23], which is considered to be the reason for the rapid drop in current density, as noted previously. From the appearance of the nano-sized depressions as early as 5 seconds after the start of anodization (Figure 3b), the formation of the porous nanostructure begins almost immediately after the formation of the oxide layer. No further conclusion regarding the origin of the initial trench formation can be reached from this observation alone since the two previous explanations offered in the literature, namely the field-assisted ejection of Ti^{4+} ions [34] and mechanical stress due to volume expansion [35], cannot be ruled out by any evidence appearing in the SEM images.

During Stage II of morphology development, the depressions continue to grow deeper into trenches, resulting in the formation of oxide nanowalls which become apparent after approximately 30 seconds of anodization (Figure 3c). Chemical dissolution of TiO_2 by H^+ and F^- ions at the oxide/electrolyte interface (Eq. 2) which should occur preferentially at crack sites presumably becomes significant during this stage and enables the initial pore sites to grow deeper. As these sites in the oxide layer become thinner due to this dissolution, the local resistance in these portions is reduced so that they undergo further preferential oxidation, leading to the formation of pore bases. The porosity of the oxide film likely increases quite rapidly during this stage. When the contribution of porosity is larger than that of the barrier oxide layer, the corresponding current that was decreasing during Stage I should now begin to increase (Figure 3c). Thus, Stage II is marked by the appearance of a minimum in the transient followed by a period of rising current.

It is important to note that the dimensions of the nanowalls as observed at the top also change as the trenches deepen during Stage II. As shown in Figure 4a, a noticeable increase in wall thickness in the first few minutes can be observed. At the same time, the nanowalls in Stage II (Figure 3c) appear to be noticeably thicker than the initial forms in Stage I (Figure 3b). This indicates that the size of the trenches is shrinking and the new oxide formed at the base

has larger dimensions than the previous layer. A possible factor for the change in nanowall dimensions is the effect of the Ti substrate since the oxide tends to grow preferentially at Ti grain boundaries [36]. This eventually leads to Stage III of morphology development where the nanowalls connect to each other and form a network of nanopores, which is observed after about 5 minutes of anodization in the case of Sample A (Figure 3d). The trenches shrink and become vertical pore channels, while the connected nanowalls form the boundaries of the nanopores.

During this stage, the vertical height of the pore walls gradually becomes non-uniform, leading to a rougher surface later in the stage (Figure 3e). At the same time, the outer diameter of the pores as they appear in the images grows larger and the pores become more circular as the reaction proceeds. As shown in Figure 4, the wall thickness and inner diameter of the nanopores as measured at the top surface both increase during this stage (between 5 to 20 minutes of anodization). Since the pore walls at the top surface are continually dissolving, the pore bases that originally form at the oxide/substrate interface eventually reach the top surface. Thus, on the basis of the trends shown in Figure 4, the pore bases formed later in the process are larger than those that appear earlier in the process. This is consistent with the equi-field strength theory [27, 37, 38], which proposes that the change in tube diameter should continue until some equilibrium is reached. As observed, the formation of larger pores would in turn cause some of them to shrink as their neighbours crowd into them and eventually degenerate into the inter-nanotube spaces observed in the final morphology (Figure 3f). As shown in Figure 4a, the thickness of the oxide walls continues to increase throughout Stage III, indicating that the oxide walls are not shrinking. This is an important observation since it is at odds with previous mechanisms that attribute the transition from nanopores to nanotubes primarily to the reduction in the volume of oxide walls either through dissolution of a fluoride-rich-layer [14], inter-pore dissolution [26] or the dehydration of a hydroxide phase [27-30]. It should also be noted that the impressions on the Ti substrates obtained after the oxide film is detached appear to be circular with an average diameter similar to the final pore diameter (Figure 3d inset) at the beginning of Stage III, which suggests that the transformation into a nanotube

array at the oxide/substrate interface has started although the top surface still appears to be an undeveloped oxide network.

The evolution of the nanotube dimensions relative to a fixed vertical position during Stage III is depicted in Figure 5a. The downward movement in the position Z_B of the pore base with time reflects that the oxide layer grows inward during anodization, while the top position Z_T corresponding to the oxide/electrolyte interface also moves downward due to the dissolution of the top layers of the oxide film. The length of the nanopores/nanotubes increases when the oxidation rate exceeds the dissolution rate (i.e., $dZ_B/dt > dZ_T/dt$). At any point during anodization, the pore bases that are just being formed are larger than those formed earlier during the process (i.e., $D_{B3} > D_{B2} > D_{B1}$). Meanwhile, examination of the change in the dimensions of the section of the nanotubes or nanopores at the same vertical height shows that the inner diameter increases with time, while the outer diameter decreases due to the continual oxide dissolution that leads to thinner walls (for example, follow the change in pore dimensions as one moves along the dashed line at $Z = Z_{B1}$ from t_1 to t_3 in Figure 5a). The film resistance decreases to a minimum and then begins to increase again during this period as the change in porosity becomes less significant and the vertical length of the nanopores/nanotubes becomes more important.

The transformation from nanopores at the top surface containing the oldest remaining pore walls to nanotubes at the bottom containing the most recently formed walls is clearly demonstrated in Figure 5b, which shows Sample A that has been anodized for 15 minutes and then fractured to reveal the nanotubes at three depths over the film thickness. At the top surface (region i in Figure 5b), the oxide film appears as an array of nanopores which are very similar in size. It is difficult to distinguish between the nanotube channel openings and the inter-nanotube spaces. However, as one moves towards the pore bases, the outer diameters become larger and the inner diameters become smaller (region ii). Eventually a close-packed array of nanotubes (region iii) can be observed closer to the bottom as the inter-tube regions shrink.

The ridges connecting adjacent nanotubes in the final morphology (Figure 2c inset) are likely remnant portions of pore walls left behind as some of the pores degenerate. Such an

explanation is also consistent with the observation that they appear only at the outer surface of the nanotubes and after anodization has been underway for some time.

Stage IV of the morphology development is marked by the complete transformation into a vertical nanotube array. The top portion of the nanostructure becomes thinner as it undergoes chemical dissolution and can be etched into thin nanowires without breaking off from the film. However, in this state, this nanowire portion would not be strong and so tend to collapse and cover the top surface of the TiO_2 film when it is removed from the electrolyte, as observed in Figure 2a. When this layer of precipitate is removed through subsequent treatment, the underlying surface has the regular nanotubular morphology as expected. This precipitation layer is not observed in samples anodized for 30 minutes or less, indicating that the top walls of the nanotubes at this point are still thick enough to retain their structure after removal from the viscous solution.

The pore walls in the nanostructure after the final stage is reached (at ~ 20 minutes in Sample A) are mostly vertical to the base since the rate at which the pore bases expand is slow compared to their growth in the vertical direction. This would lead to the tube walls appearing straight with little variation in their outer diameters from top to bottom, as observed in Figure 2c. In Figure 4b, the average pore diameter rises sharply after ~15 minutes of anodization, which coincides with the time when nanotubes rather than nanopores appear at the top surface. At this point, the inter-tube regions become much smaller than the actual pores and so are no longer counted in the measurement of pore size, leading to a much larger average in the calculation. Also shown in Figure 4, both the average pore diameter and wall thickness continue to increase, albeit at a lower rate, even near the end of the experiment at 60 minutes. This indicates that the pore base diameter continues to rise even after a close-packed morphology is reached. This agrees with a previous report that a much larger pore size can be obtained by extending the anodization time during experiments in viscous electrolytes [39]. On the other hand, a wall thickness of ~20 nm observed in Figure 4a is likely the threshold value for the oxide to maintain a stable vertical nanostructure since the top portion with thinner oxide walls tends to become thread-like and break off when removed from solution, thus leaving behind a constant wall thickness at the top.

3.2.3 Proposed mechanism

The evidence from the SEM images presented here (Figures 3 and 5) suggests that the transformation of the nanostructure from initially disconnected oxide islands to nanopores and eventually to nanotubes is driven by a single process - the change in the dimensions of the pore bases as they form during the course of anodization. The width of the trenches formed at the beginning of the process, which are believed to be the precursors of the nanopores, is mostly determined by the surface properties of the titanium substrate. This conjecture is supported by previous findings that the nanotubes can be made more uniform by surface treatment of the initial substrate [40]. On the other hand, the equilibrium inter-pore spacing which has a direct bearing on the subsequent nanopore/nanotube wall thickness is likely determined by the electrochemical conditions during anodization such as temperature and voltage. When the trenches first form, they are likely not wide enough to match the pore spacing dictated by the cell voltage and temperature. The system responds to this mismatch by increasing the size of the pores as they form at the oxide/substrate during the course of the anodization. This adjustment process is central to the transitions that occur during Stage I through to Stage IV in the proposed mechanism for evolution of the anodic TiO_2 nanostructure described below and presented schematically in Figure 6. For the purpose of the discussion that follows, pores that have a hemispherical base are denoted as major pores, while the neighboring ones that eventually diminish are referred to as minor pores.

Stage I corresponds to the formation of a barrier oxide layer, where pore sites are initiated, but the oxide film is still mostly planar. The film resistance rapidly increases as this layer grows thicker.

In Stage II, the oxide nanostructure begins to develop in the form of nanowall segments which become longer as the trenches continue to grow deeper, eventually connecting to each other to form a network with vertical pore channels. The film resistance reaches a maximum before beginning to decline as the effect of increasing porosity becomes significant.

In Stage III, the nanopore network gradually transforms into an array of nanotubes, as the newly formed pore bases grow downward with time. The diameter of the pore base, which corresponds to the outer diameter of the nanotubes in the final morphology, continues to

increase. This leads to crowding of the structure, particularly at the base, which in turn causes minor pores to collapse or degenerate into inter-tube regions. During this stage, the film resistance reaches a minimum and begins to rise again as the rise in porosity becomes more gradual and the increase in vertical length becomes significant.

In the final stage (Stage IV), the adjustment of the pore base dimensions slows down and the nanostructure grows predominately in the vertical direction. The top portion degenerates into nanowires and tends to collapse on top of the remaining oxide film upon removal from the electrolyte. The film resistance continues to increase gradually as the nanostructure grows in the vertical direction.

It is important to emphasize that the transition from nanopores to nanotubes according to the mechanism above does not occur by a process that is chemically distinct from that of the other anodization stages, unlike previously proposed models. In other models, this transition is attributed primarily to the dissolution of a fluoride-rich-layer [14], inter-pore dissolution [26] or dehydration of a hydroxide phase [27-30]. However, on the basis of our examination of the anodic TiO_2 samples by SEM (Figures 2, 3, 4 and 5), we did not found any evidence supporting the conclusion that the pre-formed oxide walls actually split.

3.3 Anodization in aqueous oxalic acid-NH_4F electrolytes

As described in the previous section, the evolution of anodic TiO_2 nanostructures formed in the ethylene glycol solution leads to the formation of distinct, close-packed nanotubes. In the following sub-sections, we present the nanostructures formed when Ti is anodized in an aqueous solution containing oxalic acid and NH_4F.

3.3.1 Anodization at 5V

Figure 7 shows the morphology of Sample B anodized in 0.05M oxalic acid containing 0.3 wt% NH_4F at 5V for 1 hour. This sample is synthesized as an example of anodization conditions which do not lead to a distinct nanotubular structure. As expected, nanotubes are not observed in the film, consistent with previous reports that this voltage is not sufficient to induce nanotubular structures [7,41]. Instead, the oxide film appears to consist of a continuous network of vertical nanopores (Figure 7a). The bottom view of the detached oxide film does not exhibit distinct nanotubes and instead appears as a rough oxide surface (Figure 7b). However, a side view of the oxide film reveals vertical channels inside of nanopores (Figure 7c). This indicates that vertically aligned nanopores are formed in the sample although the pore bases do not exhibit any noticeable geometrical order.

Morphologies corresponding to Stages I-III described in section 3.2 are observed during the anodization process, as shown in Figure 8. The nanostructures formed during anodization correspond well to those observed for Sample A except that a longer time is required for the same features to form. Shallow trenches are observed after only 5 seconds as in the previous sample, although they are much less prominent (Figure 8a). A similar morphology to that obtained after 5 s anodization of Sample A is not reached until anodization of Sample B has proceeded for ~20 s (Figure 8b), indicating a slower rate. Likewise, the extended nanowalls, interconnected oxide network and nanopore array form after ~ 1 min (Figure 8c), ~10 min (Figure 8d) and ~15 min (Figure 8e), respectively, whereas they are observed after 30 seconds, 5 min, and 10 min, respectively, in Sample A. Although not included here, the onset of Stages I, II and III in the case of Sample B lines up with the features of the corresponding current-time transient curve similarly to that observed for Sample A and shown in Figure 3. This similarity in

observed morphology indicates that the proposed evolution process occurs up until Stage III is reached.

However, Stage III of the transformation is never completed in this case. After nanopores form in Sample B, they do not develop into distinct nanotubes even after an extended anodization time of 5 hours, contrary to the behaviour observed in Sample A. As shown in Figure 8f, the growth in oxide wall thickness and pore diameter has essentially stopped after 1-2 hours of anodization, indicating that the adjustment of the pore base dimensions has also largely halted by this point. This difference from the behaviour observed for Sample A can be explained by the much lower oxidation rate at the lower applied potential of 5V. Presumably, the equilibrium inter-pore spacing for the anodization conditions of Sample B is closer to the initial spacing of trenches than it is in the case of Sample A. As a consequence, the diameter of the pore bases does not change enough for minor pores to degenerate and so the final morphology consists of an array of vertical nanopores instead of distinct nanotubes.

It should also be noted that no evidence of ridge formation is found on Sample B, which supports the proposal presented previously that the ridges originate from the remnant pore walls of degenerated nanopores. Since pores do not degenerate under the conditions for Sample B, ridge formation would not be expected to occur.

3.3.2 Anodization at 20 V

By contrast, Sample C is anodized in the same oxalic acid solution as Sample B, but at a higher applied voltage of 20 V (Figure 9). Nanotubes with comparable diameter as in Sample A form, but they are much more loosely-packed and irregular in size and shape. As with Sample B, the inner pore channels observed in the side view (Figure 9c) appear to be smooth and vertical. But unlike Sample B, the pore bases in Sample C can be easily distinguished from each other (Figure 9b). At the same time, they appear to be smaller and more irregular in shape and size than those obtained in ethylene glycol (Sample A). Likewise, from the top view, the nanotubes appear to be irregularly shaped and not close-packed. Some pores appear to have multiple compartments (see inset of Figure 9a). Periodic ridges are also found on the outer surfaces of the nanotubes (Figure 9c) and appear more prominent than those found in Sample A. Collapsed nanowires are not found on top of the sample as observed in Sample A, likely due to the faster chemical dissolution in the less viscous aqueous electrolyte that also contains a much higher H^+ concentration.

Two processes by which the morphology evolves appear to be operating in parallel during anodization of Sample C. In some regions, the four stages described in section 3.2 can be clearly observed, as shown in the SEM images in Figure 10. Sample C passes through the four stages by ~5 seconds, 20 seconds, 2 minutes and 20 minutes, respectively, of anodization, slightly faster than that observed in Sample A. The transition from an array of nanopores to distinct nanotubes in Sample C is shown in Figures 10 c-f. Once connected oxide walls have formed after 2 min anodization, the major pores becomes more circular and the minor pores begin to degenerate at ~7 min (Figure 10d). This is followed by the formation of a rough surface at ~12 min (Figure 10e) and distinct nanotubes after ~20min (Figure 10f), similar to that observed for Sample A (Figure 3e) and Sample B (Figure 8e). The space between adjacent nanotubes is much larger than in Sample A, resulting in a less closely packed nanostructure. This observation suggests that the pores formed in Sample C have reached their equilibrium size before the degenerated pores have completely disappeared. The appearance of nanotube bases that are noticeably smaller than their neighbors in Figure 9b also suggests that minor pores have not completely degenerated. The evolution of the pore diameter and wall thickness is shown in

Figure 10g. Again, no evidence of any oxide wall splitting is observed during the transition from nanopores to nanotubes.

On the other hand, the morphology appears to evolve differently in other regions, as shown in Figure 11. Following the appearance of nanowall segments at the beginning of Stage II, circular rings form in the midst of the nanowalls after about 10 seconds of anodization (Figure 11a). These oxide rings are formed in random positions and appear to have a range of sizes. As the process continues, more of these random rings form until they completely cover the substrate (Figures 11b, c), resulting in a much faster formation of nanopores. The formation of oxide rings has been observed previously during Ti anodization in an HF electrolyte [26].

As shown in Figure 11c, the arrangement of pores at this point of anodization (2 min) is similar to the final morphology after ~ 20 min in the slower evolving regions (Figure 10d). This pattern forms the basis for the final morphology in the fast growing regions, which involves oxide dissolution inside the oxide rings and their subsequent development into nanotubes. As a result, the nanopore network stage is not observed in these regions, although it is unclear whether any adjustment of the diameter of the pore bases occurs from the available information. The irregular shapes and non-uniform size distribution observed in the final morphology of Sample C may be caused by this accelerated evolution process whereby a significant number of nanotubes develop from random oxide rings rather than by the gradual evolution from a network of nanopores. This may also explain the appearance of multi-compartment nanotubes, which are not found in the other two samples. If segments of the nanowalls enclosed by the oxide rings form into vertical pore walls rather than dissolving completely, more than one compartment would form within these rings.

The causes of these variations in morphology evolution may be related to the accelerated dissolution rate and local pH fluctuations [11] during anodization, characteristic of the situation in the aqueous electrolyte. A higher dissolution rate allows the nanoporous layer of the oxide film to be completely dissolved before the bottom portion becomes close-packed. It would also speed up the dissolution of oxide from the inter-tube regions and further impede the formation of close-packed nanostructure since the adjustment of the pore base dimensions is slower in comparison. On the other hand, local pH fluctuations during the process would result in some

regions reacting faster, thus allowing the formation of oxide rings/pores at these locations. Non-homogeneities on the untreated Ti substrate could also be a contributing factor and lead to rapid and varied oxide formation.

4. Conclusions

In summary, the present work has focused on the formation of TiO_2 nanostructures during the anodization of Ti. Time-series experiments have been conducted on three samples anodized under different conditions in order to investigate the evolution of the morphology during nanostructure development. A mechanism is developed based on the geometric changes of the TiO_2 nanostructure observed during the course of anodization at 60 V in an ethylene glycol solution.

Regardless of the electrolyte composition and applied potential, a barrier oxide layer with shallow depressions initially forms during anodization, followed by the appearance of nanowall segments, which are then transformed into an inter-connected network of vertical nanopores. The transition from nanopores to nanotubes is associated with the increase in size of the major pores forming at the oxide/substrate interface that causes adjacent nanopores to degenerate into inter-tube regions. However, some differences in nanostructure formation are observed when anodization is conducted in an aqueous electrolyte (oxalic acid-NH_4F), resulting in the formation of nanopore arrays and irregular nanotubes at 5 V and 20 V, respectively.

Contrary to the assumptions in previous studies that a separate dehydration or dissolution reaction in the pore walls is responsible for the transition from nanopores to separate nanotubes, we conclude that this transformation occurs primarily due to the increase in the diameter of the pore bases forming during the course of anodization. The nanostructure evolution observed during anodization in the oxalic acid solution is still consistent with the proposed mechanism although nanotubes do not form at low applied voltage. The nanostructure development follows a similar path as observed during anodization in the ethylene glycol solution in the initial stages up to the formation of nanopores, but the final transition from nanopores to nanotubes does not occur as the equilibrium pore diameter can be reached without complete degeneration of minor pores.

Acknowledgement

The authors express their gratitude to the Natural Sciences and Engineering Research Council of Canada (NSERC) for financial support to carry out this project. The Ontario Graduate Scholarship is also acknowledged for providing a postgraduate scholarship for one of the co-authors (Y.Y.).

Reference

1. L. Kavan, M. Kalbác, M. Zukalová, I. Exnar, V. Lorenzen, R. Nesper and M. Graetzel, *Chemistry of Materials*, 2004, **16**, 477.
2. V. Galstyan, E. Comini, G. Faglia and G. Sberveglieri, *Sensors*, 2013, **13**, 14813.
3. Y. Wu, J. Yu, H. M. Liu and B. Q. Xu, *Journal of Nanoscience and Nanotechnology*, 2010, **10**, 6707.
4. J. Qu and C. Lai, *Journal of Nanomaterials,* 2013, **2013**, 762730.
5. Y. Li, X.-Y. Yang, Y. Feng, Z.-Y. Yuan and B.-L. Su, *Critical Reviews in Solid State and Materials Sciences*, 2012, **37**, 1.
6. V. Zwilling, M. Aucouturier and E. Darque-Ceretti, *Electrochimica Acta*, 1999, **45**, 921.
7. D. Gong, C. A. Grimes, O. K. Varghese, W. Hu, R. S. Singh, Z. Chen and E. C. Dickey, *Journal of Materials Research*, 2001, **16**, 3331.
8. Z. Lockman, S. Ismail, S. Sreekantan, L. Schmidt-Mende and J. L. MacManus-Driscoll, *Nanotechnology*, 2010, **21**, 055601.
9. C. Richter, Z. Wu, E. Panaitescu, R. J. Willey and L. Menon, *Advanced Materials*, 2007, **19,** 946.
10. C. Richter, E. Panaitescu, R. Willey and L. Menon, *Journal of Materials Research*, 2007, **22**, 1624.
11. J. M. Macak, H. Tsuchiya, L. Taveira, S. Aldabergerova and P. Schmuki, Angewandte Chemie International Edition, 2005, **44**, 7463.
12. K. Shankar, G. K. Mor, H. E. Prakasam, S. Yoriya, M. Paulose, O. K. Varghese and C. A. Grimes, *Nanotechnology,* 2007, **18**, 065707.

13. Z. Su and W. Zhou, *Journal of Materials Chemistry*, 2011, **21**, 8955.
14. A. Ghicov and P. Schmuki, *Chemical Communications*, 2009, **20**, 2791.
15. L. Yang, S. Luo, Q. Cai and S. Yao, *Chinese Science Bulletin*, 2010, **55**, 331.
16. S. P. Albu, P. Roy, S. Virtanen and P. Schmuki, *Israel Journal of Chemistry*, 2010, **50**, 453.
17. D. Regonini, C.R. Bowen, A. Jaroenworaluck and R. Stevens, 2013, *Materials Science and Engineering R: Reports*, **74**, 377.
18. Z. Su, M. Bühl, and W. Zhou, *Journal of the American Chemical Society*, 2009, **131**, 8697-8702.
19. P. Skeldon, G. E. Thompson, S. J. Garcia-Vergara, L. Iglesias-Rubianes and C. E. Blanco-Pinzon, *Electrochemical and Solid-State Letters*, 2006, **9**, B47.
20. S. J. Garcia-Vergara, P. Skeldon, G. E. Thompson and H. Habazaki, *Electrochimica Acta*, 2006, **52**, 681.
21. D. J. LeClere, A. Velota, P. Skeldon, G. E. Thompson, S. Berger, J. Kunze, P. Schmuki, H. Habazaki and S. Nagata, *Journal of the Electrochemical Society*, 2008, **155**, C487.
22. H. Habazaki, M.Uozumi, H. Konno, K. Shimizu, S. Nagata, K. Takayama, Y.Oda, P. Skeldon, and G. E. Thompson, *Journal of the Electrochemical Society*, 2005, **152**, B263.
23. S. Berger, J. Kunze, P. Schmuki, D. LeClere, A. T. Valota, P. Skeldon and G. E. Thompson, *Electrochimica Acta,* 2009, **54**, 5942.
24. S. P. Albu and P. Schmuki, *Electrochimica Acta*, 2013, **91**, 90.
25. D.-J. Yang, H.-G. Kim, S.-J. Cho, and W.-Y. Choi, *Materials Letters,* 2008, **62**, 775.
26. G.K. Mor and O. K. Varghese, *J. Mater. Res.*, 2003, **18**, 2588-2593.
27. Z. Su and W. Zhou, *Journal of Materials Chemistry*, 2009, **19**, 2301.
28. A. Jaroenworaluck, D. Regonini, C. R. Bowen, R. Stevens, and D. Allsopp, 2007, *Journal of materials science*, **42**, 6729.
29. Y. Z. Huang and D. J. Blackwood, *Electrochimica acta*, 2005, **51**, 1099.
30. B. Chen, J. Hou and K. Lu, *Langmuir,* 2013, **29**, 5911.
31. H. Habazaki, K. Fushimi, K. Shimizu, P. Skeldon, and G.E. Thompson, *Electrochemistry Communications*, 2007, **9**, 1222-1227.

32. D. Regonini, C. R. Bowen, R. Stevens, D. Allsopp and A. Jaroenworaluck, 2007, *Physica Status Solidi (A)*, **204**, 1814.
33. D. Regonini, A. Satka, D. W. Allsopp, A. Jaroenworaluck, R. Stevens and C. R. Bowen, *Journal of Nanoscience and Nanotechnology*, 2009, **9**, 4410.
34. P. Roy, S. Berger and P. Schmuki, *Angewandte Chemie International Edition*, 2011, **50**, 2904.
35. Q.Van Overmeere, F. Blaffart and J. Proost, *Electrochemistry Communications*, 2010, **12**, 1174.
36. L. Su, Y. X. Gan, and J. G. Lawrence, *Nanosci. Nanotechnol. Lett.* 2012, **4**, 520-529.
37. Z. Su and W. Zhou, *Journal of Materials Chemistry*, 2011, **21**, 357.
38. Z. Su and W. Zhou, *Advanced Materials*, 2008, **20**, 3663-3667.
39. S. Yoriya and C. A. Grimes, *Langmuir*, 2009, **26**, 417-420.
40. K. Lu, Z. Tian, and J. A. Geldmeier, *Electrochimica Acta*, 2011, **56**, 6014– 6020.
41. Q. Cai, M. Paulose, O. K. Varghese and C. A. Grimes, *Journal of Materials Research*, 2005, **20**, 230.

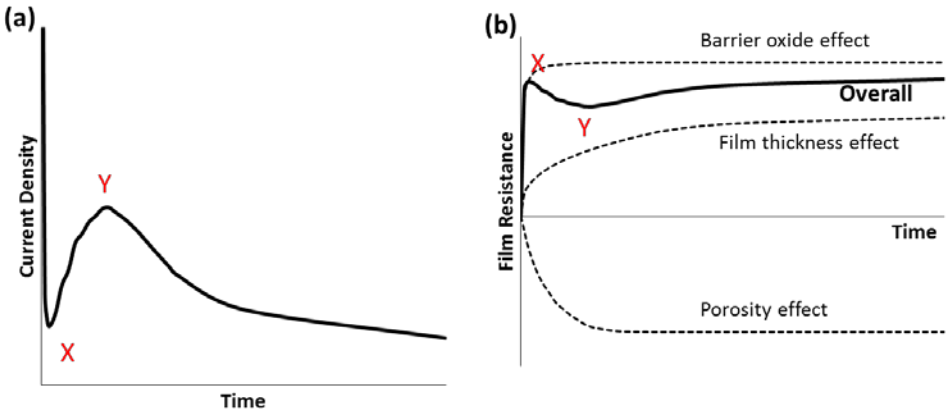

Figure 1: (a) Typical current-time transient and (b) Evolution of film resistance during the initial stages of anodization. Axes are not to scale.

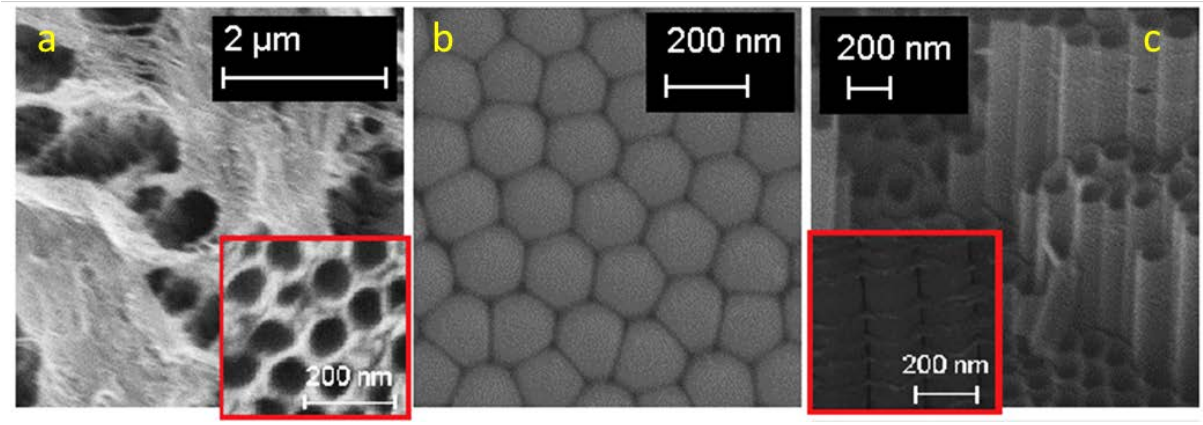

Figure 2: SEM images of Sample A (ethylene glycol / 0.3 wt% NH_4F / 2 vol% H_2O, 60 V) formed after one hour of anodization: (a) top, (b) bottom, (c) side view.

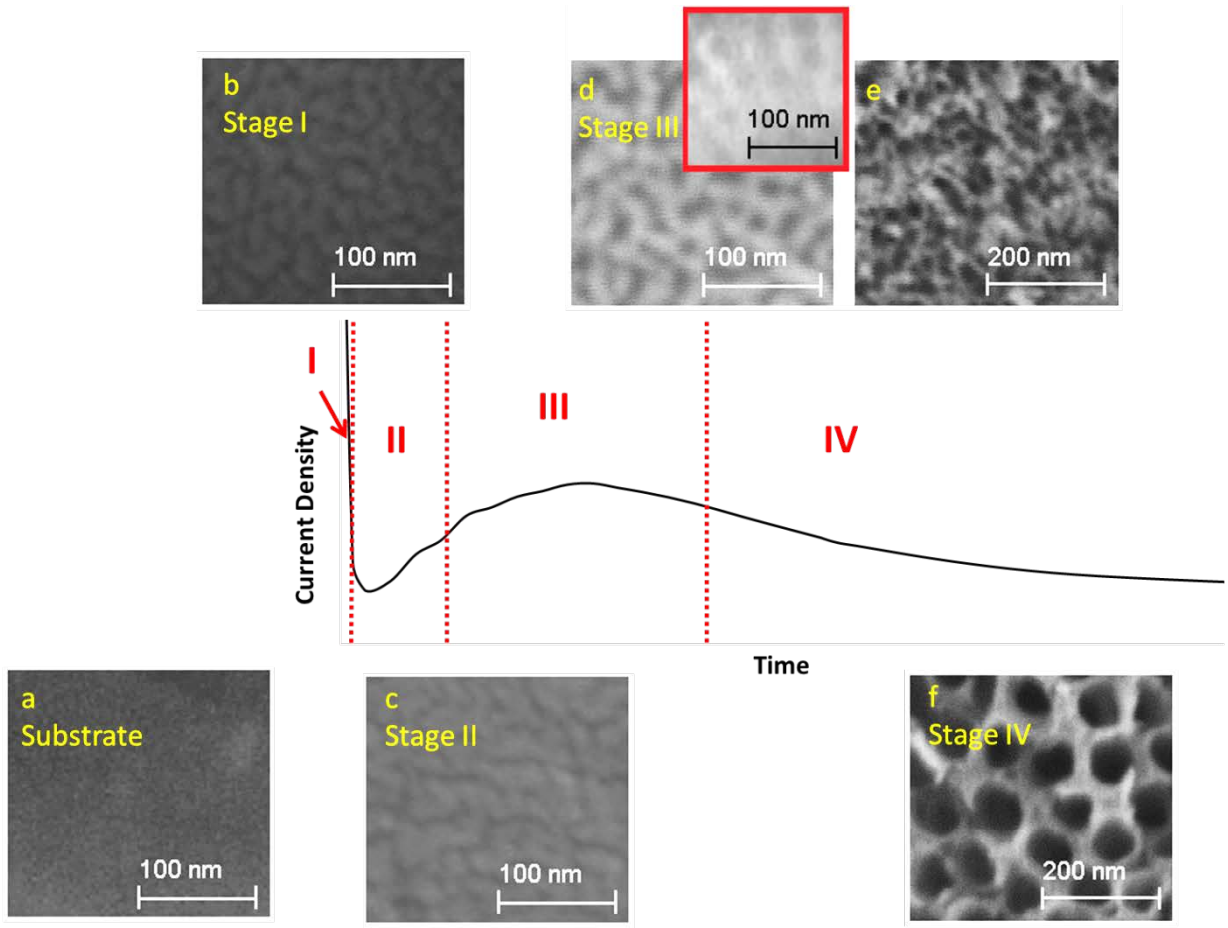

Figure 3: Stages in the morphology evolution of Sample A (ethylene glycol / 0.3 wt% NH_4F / 2 vol% H_2O, 60 V). Typical morphology at each stage as observed from the top is shown in the SEM images: (a) 0s (Ti substrate), (b) 5s, (c) 30s, (d) 5 min, (e) 10 min, and (f) 30 min. The inset in (d) shows the impression left on the Ti substrate after the oxide film is removed after 5 min.

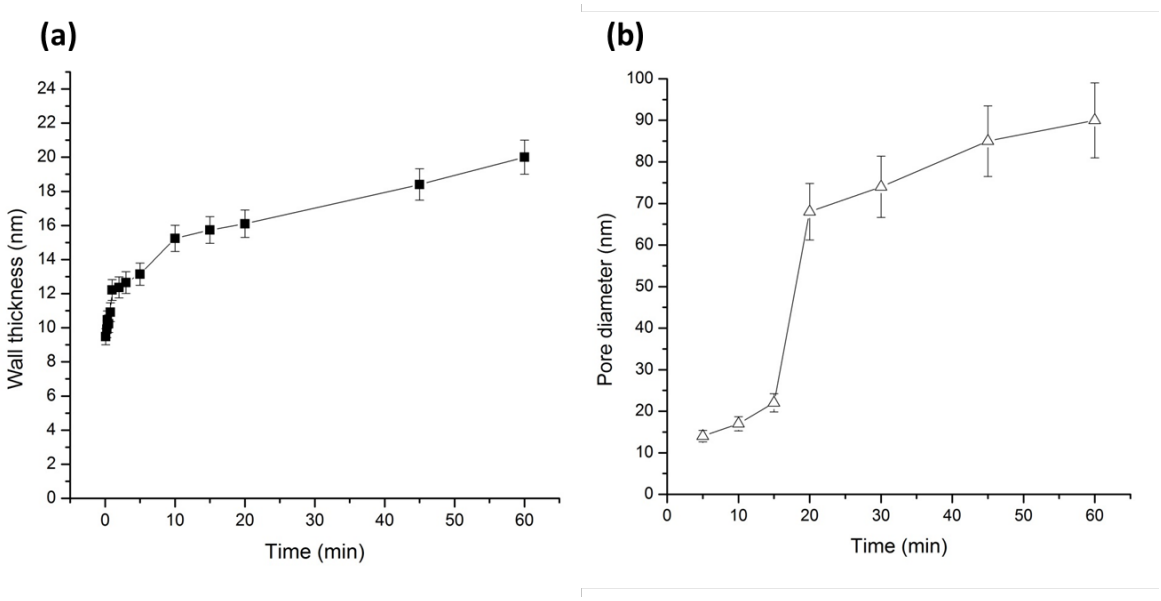

Figure 4: Evolution of (a) wall thickness and (b) pore diameter in Sample A (ethylene glycol / 0.3 wt% NH_4F / 2 vol% H_2O, 60 V). The sharp rise in (b) signifies the complete transformation into nanotubular array.

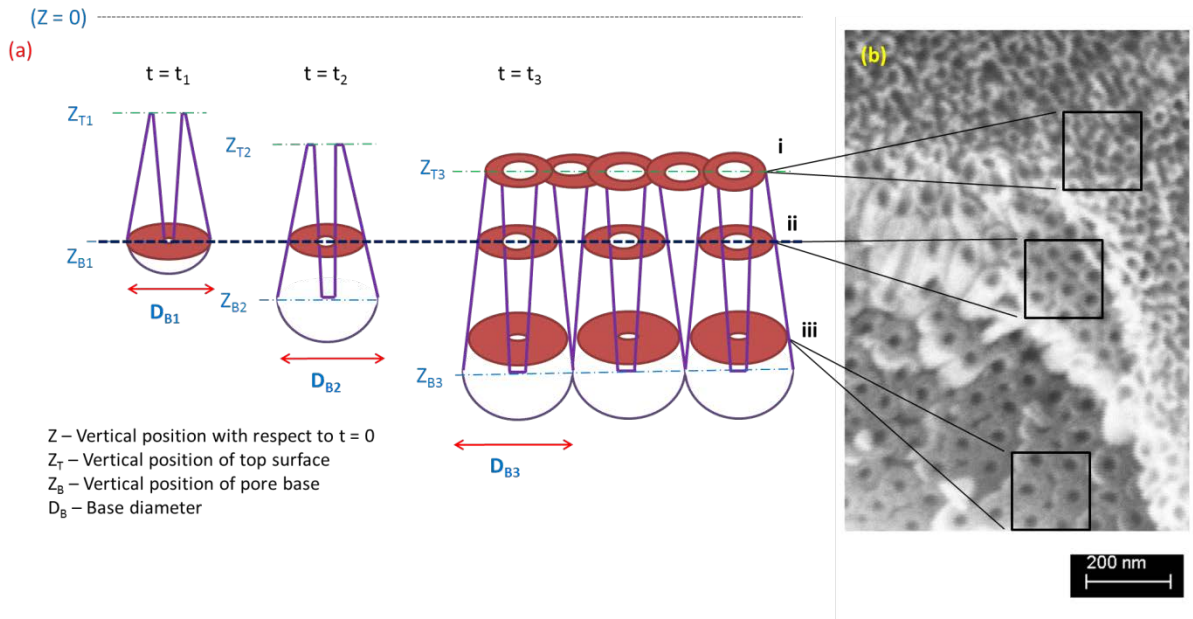

Figure 5: (a) Schematic showing the evolution of nanotube dimensions relative to a fixed vertical position; (b) SEM images of Sample A (ethylene glycol / 0.3 wt% NH_4F / 2 vol% H_2O, 60 V) after 15 minutes of anodization with layers at different heights labelled: (i) top nanoporous surface, (ii) nanotube layer and (iii) more newly formed nanotube layer with larger outer diameters, smaller inner diameters and smaller inter-tube spacing.

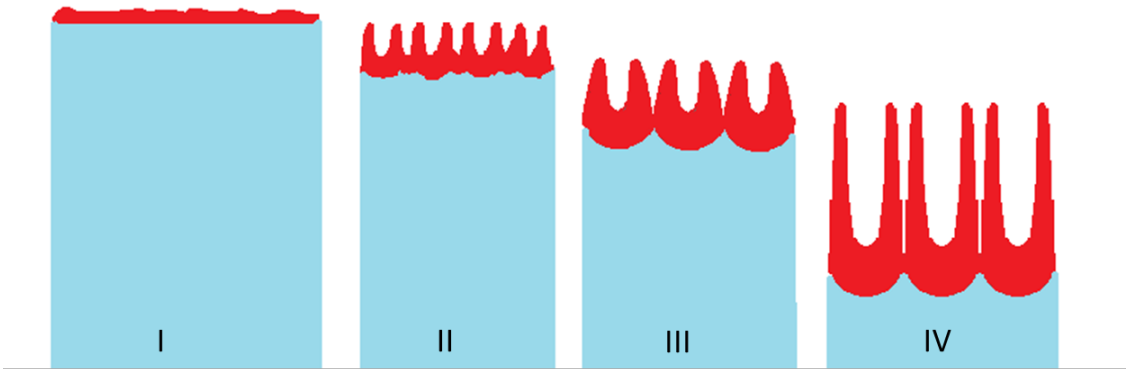

Figure 6: Schematic of TiO_2 nanotube formation mechanisms: (I) barrier oxide film, (II) nanowalls and trenches, (III) network of nanopores, (IV) nanotubes.

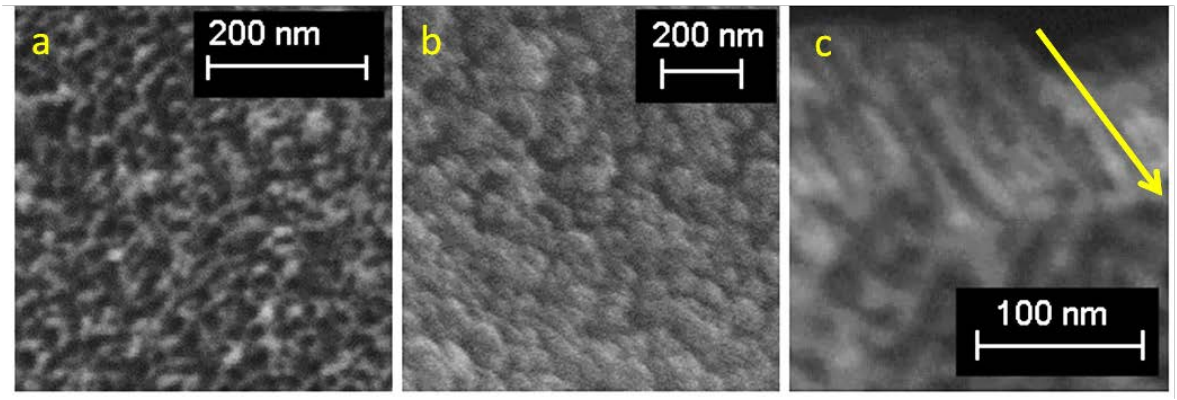

Figure 7: SEM images of Sample B (0.05M oxalic acid / 0.3 wt% NH_4F, 5V) formed after one hour of anodization: (a) top, (b) bottom, (c) side view (with nanopore direction labelled).

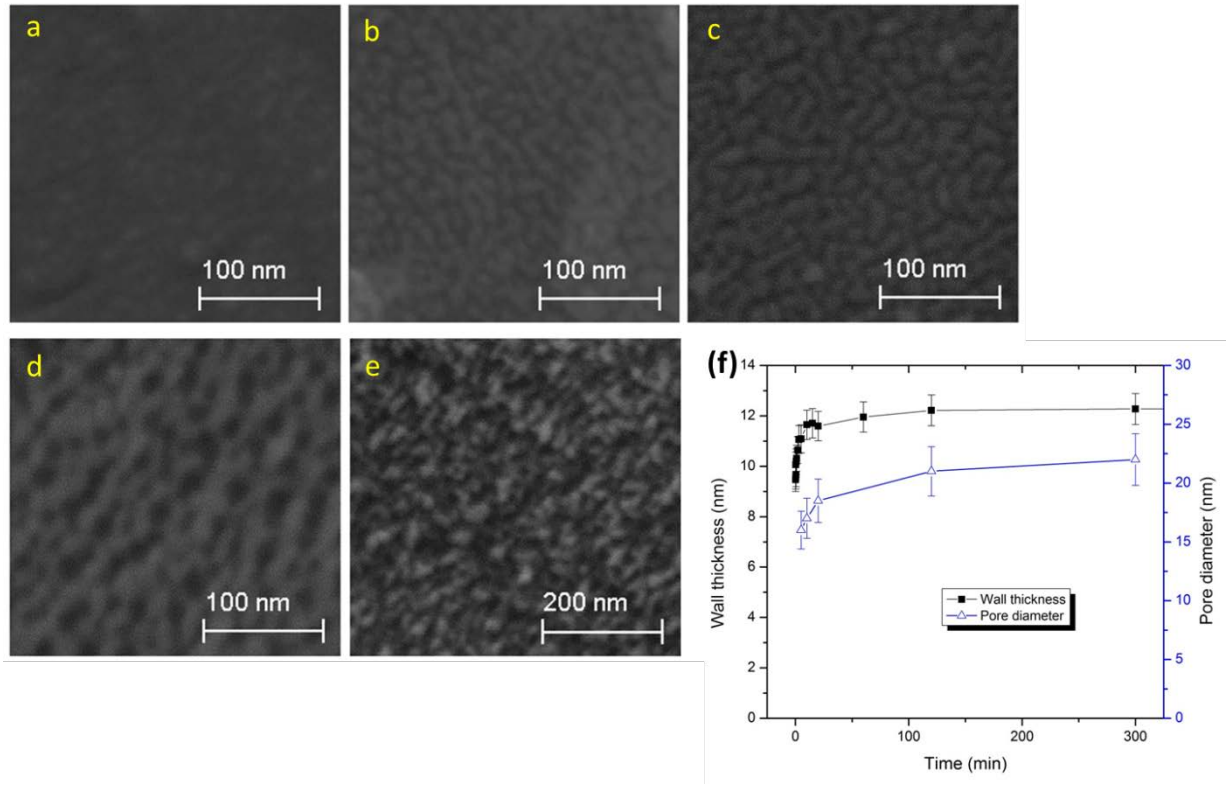

Figure 8: : SEM images of Sample B (0.05M oxalic acid / 0.3 wt% NH_4F, 5V) after (a) 5s, (b) 20s, (c) 1 min, (d) 10 min and (e) 15 min. The evolution of pore diameter and wall thickness is shown in (f).

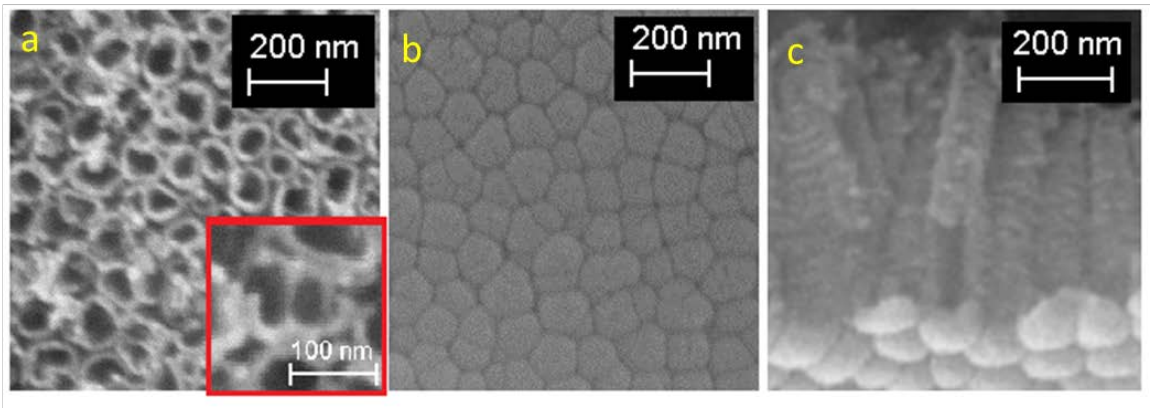

Figure 9: : SEM images of Sample C (0.05M oxalic acid / 0.3 wt% NH_4F, 20V) formed after one hour of anodization: (a) top, (b) bottom, (c) side view.

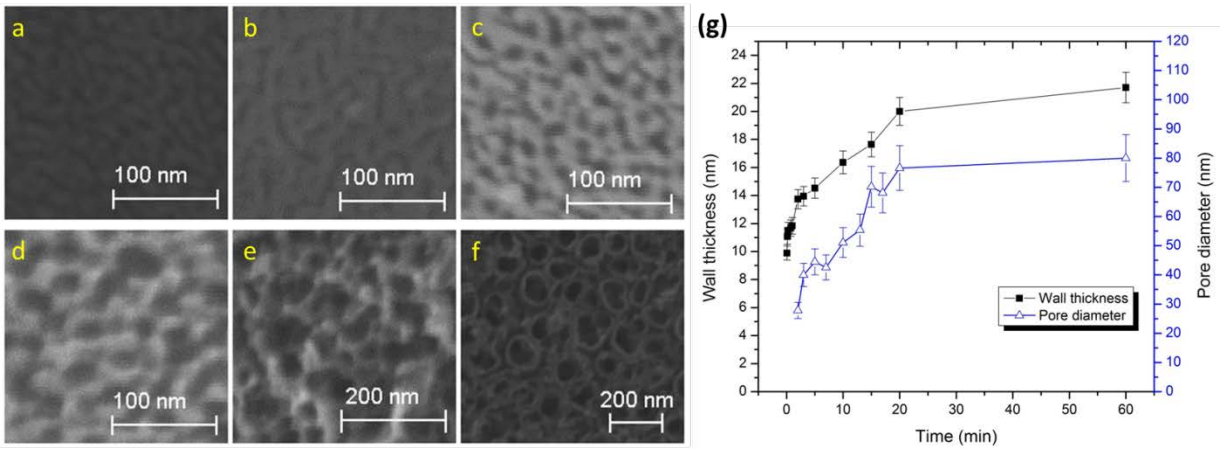

Figure 10: SEM images of Sample C (0.05M oxalic acid / 0.3 wt% NH_4F, 20V) after (a) 5s, (b) 20s, (c) 2 min, (d) 7 min, (e) 12 min and (f) 20 min. The evolution of pore diameter and wall thickness is shown in (g).

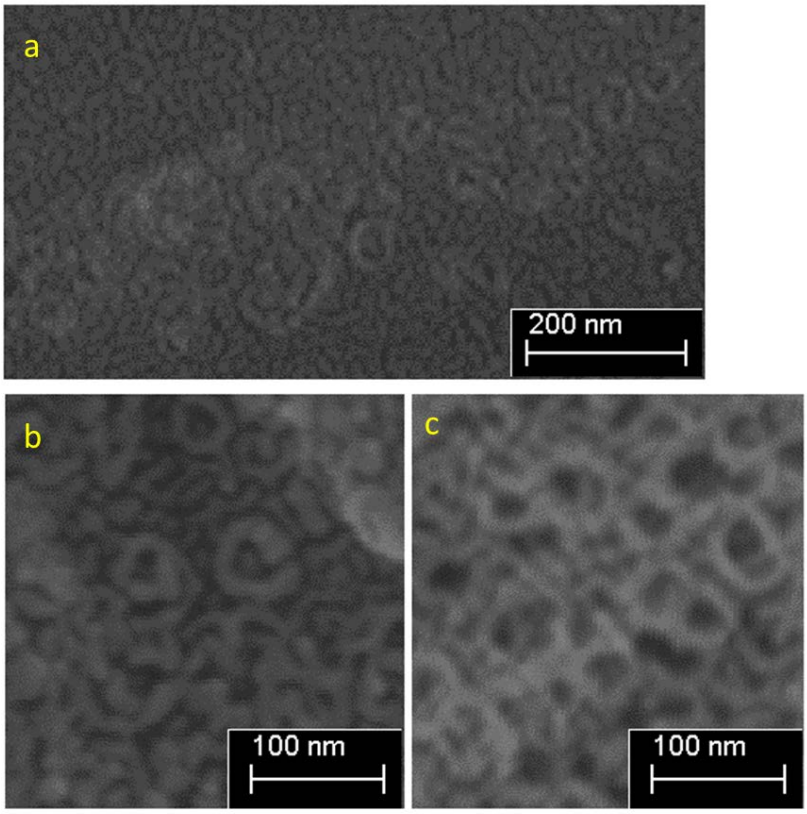

Figure 11: Morphology evolution in the irregular regions of Sample C observed at (a) 10s, (b) 15s and (c) 2 min.